SPACE SCIENCES

Universal energy limits of radiation belts in planetary and brown dwarf magnetospheric systems

Drew L. Turner[1]*, Savvas Raptis[1], Adnane Osmane[2], Arika Egan[1], George Clark[1], Tom Nordheim[1], Leonardo Regoli[1], Aleksandr Y. Ukhorskiy[1]

Radiation belts are regions of magnetically trapped particle radiation found around all of the sufficiently magnetized planets in the Solar System and recently also observed around brown dwarfs, yet despite their ubiquity, there is not yet a general theory or model to predict the uppermost energy limits that any particular magnetospheric system's radiation belts can attain. By considering only the most fundamental loss processes, a model and corresponding theory are developed that successfully bound and explain the maximum observed energies of all documented radiation belt systems. This approach yields a relatively simple function for the uppermost energy limit that depends on only the surface magnetic field strength of the system. The model predicts an energy limit for all radiation belt systems that asymptotes at 7 ± 2 teraelectronvolts (TeV) (for protons and electrons), offering intriguing, previously unrecognized insight on potential sources of galactic cosmic rays. This model is also applied to an exoplanetary system, demonstrating that the planet is likely a synchrotron emitter and showcasing the model's use for identifying candidate targets for synchrotron-emitting astrophysical systems and revealing details critical to habitability at those remote worlds.

INTRODUCTION

Magnetospheric systems, such as the space environments surrounding Earth and Jupiter dominated by intrinsic planetary magnetic fields, are able to trap charged particles, concentrate them at very high intensities, and accelerate them to relativistic energies ($v \sim c$). Earth's radiation belts boast intense populations of trapped protons and heavy ions up to several gigaelectronvolts (GeV) (*1*) and electrons up to ≥15 MeV (*2*); meanwhile, Jupiter, with its strong internal dynamo and enormous magnetospheric system, retains intense populations of positive ions and electrons up to at least 2.5 GeV and 100 MeV, respectively (*3*, *4*). Every sufficiently magnetized planet in the Solar System boasts radiation belts, and radiation belts have now also been observed by imaging synchrotron emissions from a brown dwarf magnetospheric system (*5*). This implies that, provided adequate conditions, radiation belts are ubiquitous in magnetospheric systems, both planetary and stellar, throughout the cosmos. Considering that, a generalized model is developed to estimate the upper energy limits on any radiation belt system. This model successfully bounds the upper energies at every observed radiation belt system throughout the Solar System and beyond and even offers predictive capability for the uppermost electron energies observed at Mercury, Earth, Jupiter, Saturn, Uranus, and Neptune. Applied to brown dwarfs, the model can explain the synchrotron emissions from ultracool dwarf LSRJ1835 + 3295 (*5*, *6*) and also predict the maximum possible electron and proton energies at that system as ~7 teraelectronvolts (TeV), which the model produces as a universal asymptotic limit for uppermost energy possible in planetary to brown dwarf radiation belt systems and is consistent with the unexplained break in the cosmic ray electron (and positron) spectrum around ~1 TeV (*7*, *8*). Furthermore, the model can be applied to exoplanetary systems, offering predictive capability to prioritize which exoplanets may be synchrotron emitters and revealing details of their potential for habitability.

Intrinsic magnetic (B) fields are generated by internal dynamo processes within large, spinning planets and stars (and even some moons), and the resulting fields tend to be dominated by a large dipole moment. In a sufficiently strong, dipole-like B field, energetic charged particles (i.e., particles within the suprathermal to relativistic tails of collisionless plasma distributions) can be effectively trapped in the field by the Lorentz force, which results in three characteristic periodic motions (*9*): (i) gyration around the field lines, (ii) bounce between mirror points along the field lines, and (iii) azimuthal drift perpendicular to field lines around the full system. Hamiltonian action integrals associated with each of those motions can be derived into a set of three adiabatic invariants. The invariants remain conserved so long as the underlying B field is not changing on timescales or spatial scales comparable to the periods or scales, respectively, of the corresponding motions. The first invariant, associated with the gyromotion and magnetic rigidity, is the most difficult to invalidate, and the conservation of this invariant, $\mathrm{Mu} \propto K/B$, where K is kinetic energy, results in betatron acceleration or deceleration provided increases or decreases, respectively, in the ambient B field. The conservation of the second adiabatic invariant, associated with the bounce motion, results in Fermi-type acceleration or deceleration. Meanwhile, the third invariant, associated with azimuthal drift around the system, is the easiest to invalidate, resulting in radial transport within the system. Collectively, these invariants are critical to all acceleration, loss, and transport processes in radiation belt systems (*10*).

A number of critical processes have been identified for radiation belt sources, acceleration, losses, and transport, particularly at Earth (*11*–*13*). Here, we develop a model that is independent of any particular system's source, acceleration, or transport processes. Instead, this model focuses only on the universal limiting loss factors of trapped energetic particles in radiation belt systems. Those limiting factors include: (i) the gyrosounding limit, (ii) the magnetic rigidity limit, and (iii) the synchrotron limit. The gyrosounding limit is the simplest, both physically and comprehensively, in that particles are assured to be lost once their energy and corresponding gyroradius are so large that the gyromotion intersects the host celestial body

[1]Johns Hopkins Applied Physics Laboratory, Laurel, MD, USA. [2]University of Helsinki, Helsinki, Finland.
*Corresponding author. Email: drew.turner@jhuapl.edu

(i.e., the planet or star). The magnetic rigidity limit is associated with conservation of the first adiabatic invariant; when a particle's gyroradius becomes comparable to the radius of curvature of the background B field, the first invariant is broken and the particle is randomly scattered (*14*). This scattering will ultimately result in particles rapidly "precipitating" down field lines and into the host celestial body, where they will be absorbed and lost due to collisions in dense media. The synchrotron limit is only relevant for the highest energy, highly relativistic particles, which achieve energies where their gyromotion in the *B* field results in the rapid emission of energy in the form of synchrotron radiation, ultimately limiting their maximum obtainable energy.

Combined, these loss terms, and particularly the gyrosounding and synchrotron terms, represent fundamental limits and hard sinks negating the effects of any particle acceleration and/or sources within a radiation belt system. The synchrotron limit is self-limiting and asymptotic; once particles hit the synchrotron limit, where their synchrotron energy loss timescale is on the same order as any energy they could gain while conserving adiabaticity, they lose energy just as fast as they can gain it (note that the synchrotron energy loss function is proportional to K^4). Meanwhile, gyrosounding is an absolutely hard physical limit, above which particles are ensured to be entirely lost to the system by either a collision with the host body itself or nonadiabatic outward transport and escape to the outer boundary (e.g., the dayside magnetopause in typical planetary magnetospheres). This model does not consider outer boundaries explicitly, which may be a limiting factor for very small systems (i.e., considerably smaller than Mercury), highly compressed systems with small "daysides" and/or systems where a magnetotail-like configuration starts at very low *L*-shells. Stated differently, these loss limits apply regardless of the nature of competing acceleration and/or source processes. Thus, the uppermost energy limits within planetary to brown dwarf radiation belt systems are simply a function of these loss terms and are independent of any competing acceleration and/or source processes within a system; however, to determine the uppermost energy attainable at any particular system—which, if our theory is correct, must always be either at or below the uppermost energy limit—all of the substantial source, loss, acceleration, and transport mechanisms must also be accounted for in that system.

RESULTS

Our model considers the following inputs: the host celestial body's (i) size (i.e., planetary or stellar radius), (ii) *B* field dipole moment magnitude, (iii) spin rate, and (iv) magnetospheric plasma density as well as a range of Mu for a particular particle species (e.g., electrons, protons, alphas, etc.). Using the approximation of a dipole field, the model is fully analytical yet only applicable in relatively close proximity to the host body (i.e., at relatively low *L*, where *L* is a magnetic field line coordinate specified as the radial distance from the center of the body to a point in the magnetic equatorial plane in units of planetary radii). The close proximity approximation is reasonable, however, considering that charged particle radiation coalesces and is most intense close to the host celestial body. The simplifying assumptions are reasonable, but some consideration of their implications reveals some interesting aspects. First, the centered-dipole approximation further ensures that the limits are truly upper limits, since asymmetric and higher order–term *B* fields contribute to additional loss and scattering from a system, such as larger drift-loss cones and perturbations to stable trapping as was demonstrated for protons in the radiation belts at Uranus (*15*). For systems that are dipolar but have a significant dipole offset, resulting in off-centered and asymmetric field geometries, the drift loss cone (*16*) becomes larger, effectively resulting in an increased planetary radius and enhancing the gyrosounding loss term, described below. Thus, those systems with nondipolar and/or asymmetric, off-centered fields should have lower actual energies than what this model would predict.

With those inputs, particle energies can be derived as a function of *L*-shell and Mu assuming conservation of the first adiabatic invariant, as shown in the underlying color and contours in Fig. 1. Here, we only show results for particles in the magnetic equatorial plane where the particles' pitch angle (i.e., α, the angle between the particle velocity and local *B* field vectors) is 90°; these particles are the most stably trapped and can attain the highest intensities at any

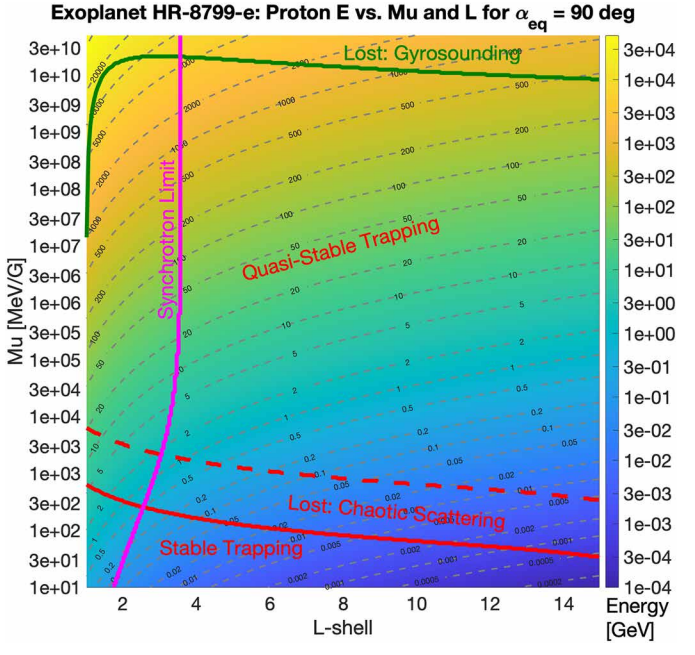

Fig. 1. Example model output for radiation belts at exoplanet HR-8799-e. Energy limit model results applied for equatorially mirroring protons in a hypothetical radiation belt system at exoplanet HR-8799-e. Proton energy is plotted in color as a function of *L*-shell and first adiabatic invariant, Mu, with constant energy contours (in units [GeV]) shown with dashed gray lines. Overplotted in this [*L*, Mu, *E*] state space are curves corresponding to the limit factors discussed in the text: (i) chaotic scattering due to loss of magnetic rigidity (violation of the first adiabatic invariant) in red; (ii) gyrosounding limit, in which a particle's gyroradius is as large as the *L*-shell resulting in sudden loss from the system, in green; and (iii) the synchrotron limit, in which the energy loss timescale by synchrotron emissions is on the same order as the particle's drift period, in pink. Essentially, anything above the green line, to the left of the pink line, or between the red solid and dashed lines should be lost very quickly from the system. However, any particles in the regions labeled "stable trapping" or "quasi-stable trapping" should be able to remain and accumulate within this radiation belt system. Whether a system can attain its theoretical upper energy limit ultimately depends on the different source, acceleration, transport, and loss processes active within the system, so this model offers an estimate of the uppermost energy limits possible within a radiation belt system plus insight on whether a system might be an active emitter of synchrotron radiation. Note that for ease of reproducibility and open clarity on the underlying model, the MATLAB code used to generate this plot and the corresponding data are included in Materials and Methods.

particular energy (or Mu) in any dipole-like magnetospheric system. However, this model does include all stably trapped pitch angles outside of the loss cone(s), and in the Supplementary Materials, we demonstrate how $\alpha = 90°$ is representative of other pitch angles; the uppermost energies attained are comparable across all pitch angles for a fixed Mu because of the nature of the loss processes. Next, the universal limits are included as a function of location in the B field and corresponding particle energy. The gyroradius, $\rho = \gamma m_0 v_\perp / qB$, is calculated and converted to units of planetary radius, such that once $\rho \sim L$, we qualify a particle as having reached the gyrosounding limit and being lost from the system.

For the rigidity limit, the radius of curvature of the background B field, R_{cB}, is also required, and for this, we also consider the centrifugal stretching of magnetospheric B fields due to rapid rotation (see Materials and Methods). In rapidly rotating systems, B fields are pulled radially outward by centrifugal forces, resulting in a reduction of the equatorial B field radius of curvature and the formation of "magnetodisks" at systems such as Jupiter and Saturn (*17*). The model does not consider any additional modifications to the B field, such as those from magnetopause or magnetotail current systems. Magnetic rigidity is a complicated factor. Based on theory (*18*–*20*), simulations (*21*), and supporting observations (*22*), a critical term discerning particles that are stably trapped, scattering chaotically, or quasi-stably trapped is $\kappa^2 = R_{cB}/\rho$. When $\rho \ll R_{cB}$ (i.e., κ^2 is very large), particles are stably trapped and fully adiabatic; that is, in this "stable" regime, particles successfully undergo all three characteristic periodic motions that enable trapping in a magnetic bottle configuration: gyration, bounce, and drift. When $\kappa^2 \leq 1$, particles undergo a quasi-stable bounce motion in which the trajectory is adiabatic away from the minimum in R_{cB} along the field lines but goes ballistic around the minimum in R_{cB} (*18*, *19*). Stated differently, particles undergoing quasi-stable motion are stably trapped near their mirror points at higher magnetic latitudes along field lines but go through a relatively untrapped, ballistic motion at low latitudes around the magnetic equatorial plane. In a critical regime $1 < \kappa^2 < {\kappa_{cr}}^2$, particles behave chaotically in the field and reach a strong pitch angle diffusion limit, in which they scatter very rapidly into the loss cone of the host body (i.e., where the mirror points fall to altitudes below the collisional regime of the host and particles are lost). Based on theory and supporting simulations, ${\kappa_{cr}}^2$ typically ranges between 3 and 33, with an ideal value of ~8 (*18*). For our model, we consider a range of κ^2 as a function of energy and L-shell and consistent with theory in which particles are lost rapidly from a magnetospheric system.

Last, for the synchrotron limit, the energy loss rate is calculated as $f_\rho K_{sync} \propto K^4/\rho$, where f_ρ is the gyrofrequency, and when the e-folding (i.e., the time at which the energy drops by a factor of e) timescale of the energy loss by synchrotron emissions becomes comparable to the relativistic drift period, $T_{drift} \propto {R_p}^2 qB / (\gamma m_0 L)$, where R_p is planetary radius and q is a particle's charge, particles are considered to have hit an asymptotic upper energy limit and can no longer be accelerated in the system. Figure 1 shows this model applied to protons in the HR-8799-e exoplanetary system as an example case that details each of those limits and how they appear in the [L, Mu, E] state space.

There are seven magnetospheric systems within the Solar System—Mercury, Earth, Ganymede, Jupiter, Saturn, Uranus, and Neptune—and applying this model at each showcases its effectiveness at predicting the uppermost energy limits for radiation belt systems. For electrons, the model successfully bounds the uppermost energies that have been observed or estimated at each magnetospheric world. For protons (and heavier ions), the model also successfully bounds the observed upper energy limits at Mercury, Earth, Jupiter (including oxygen ions), Ganymede, Saturn, Uranus, and Neptune. Figure 2 shows the results for electrons and ions, respectively, at Mercury, Earth, and Jupiter (see plots for other systems in the supporting material). All of the proton and electron observations are within the upper energy limits for gyrosounding and stable trapping, respectively, as predicted by the model, and at Jupiter, the model also accurately estimates the peak of electron synchrotron emissions at $L \sim 1.3$. It seems as though the rigidity limit is most critical to electrons while the gyrosounding and/or synchrotron limits are most critical to protons and heavier ions, although ultimately, this is also dependent on the sources and source energies of particles at each system. For example, to enable electrons at Earth to get into the quasi-stable trapping regime, there would need to be either (i) some sufficient source of electrons at >1 MeV at $L > 10$, including some inward transport process to further accelerate them or (ii) direct injections on the order of 10 MeV directly and routinely into $L < 6$, but there are no known mechanisms that do that. However, at Ganymede, a moon-magnetosphere system embedded entirely within Jupiter's own magnetosphere, there is a sufficient source of MeV electrons from the Jovian radiation belts to provide an external supply at approximately MeV electrons directly into the quasi-stable trapping regime at that system (*23*). Jupiter's observed limits are ultimately bounded by the performance ranges of observatories that have probed that system, but for Neptune and Uranus and to some extent Saturn, those systems might be more limited by a lack of particle sources in the system [e.g., Neptune (*24*)] and/or additional, dominant loss processes [e.g., Saturn and its ring system (*25*)]. Ultimately, the observed maximum energies of radiation belt particles all fall below the predicted maxima from this model in all of the systems where observations are available (including both remote sensing and in situ measurements), as shown in Fig. 3.

It is intriguing that, at least for electrons, each of the systems appears to reach its upper energy limit based on rigidity; that is, for all of the observed systems, electrons that reach or exceed the stable trapping limit regardless of different source, acceleration, transport, and loss processes are active. This implies that regardless of either universal or distinctive source, acceleration, loss, and transport processes within any particular radiation belt system, if the source, acceleration, transport, and loss conditions are appropriate, then a system can and does indeed reach those uppermost stable-trapping energy limits for electrons. Protons and ions, which in the Solar System have more abundant external sources at higher energies compared to electrons, not only seem more readily able to extend above the ${\kappa_{cr}}^2$ limit but also seem ultimately more limited by loss processes. For protons, magnetotails and cosmic rays both provide sufficient sources and direct injection of protons right into the quasi-stable trapping regime, so unlike for electrons everywhere but Ganymede, the chaotic scattering regime due to loss of rigidity is not a hard limit for protons throughout the Solar System's magnetospheres. Based on these results, this model offers distinct promise for application to astrophysical radiation belt systems elsewhere in the cosmos.

Applying the model to the ultracool brown dwarf system, LSRJ1835+3259 (*5*), the model successfully reproduces the reported ≥15-MeV electrons [Climent *et al.* (*6*) reported 21 MeV] synchrotron emitting at $L \sim 12$ in the system. For this estimate, the observed (*5*, *26*) 1- to 3-hour spin period and ~5-kG surface B field strength were used. A stellar radius of 70,000 km was assumed (*5*), and the plasma mass density within the system was estimated at 2×10^{-21} kg/m^3 [i.e., ~1% of Jupiter's plasma density based on (*27*)]. With those

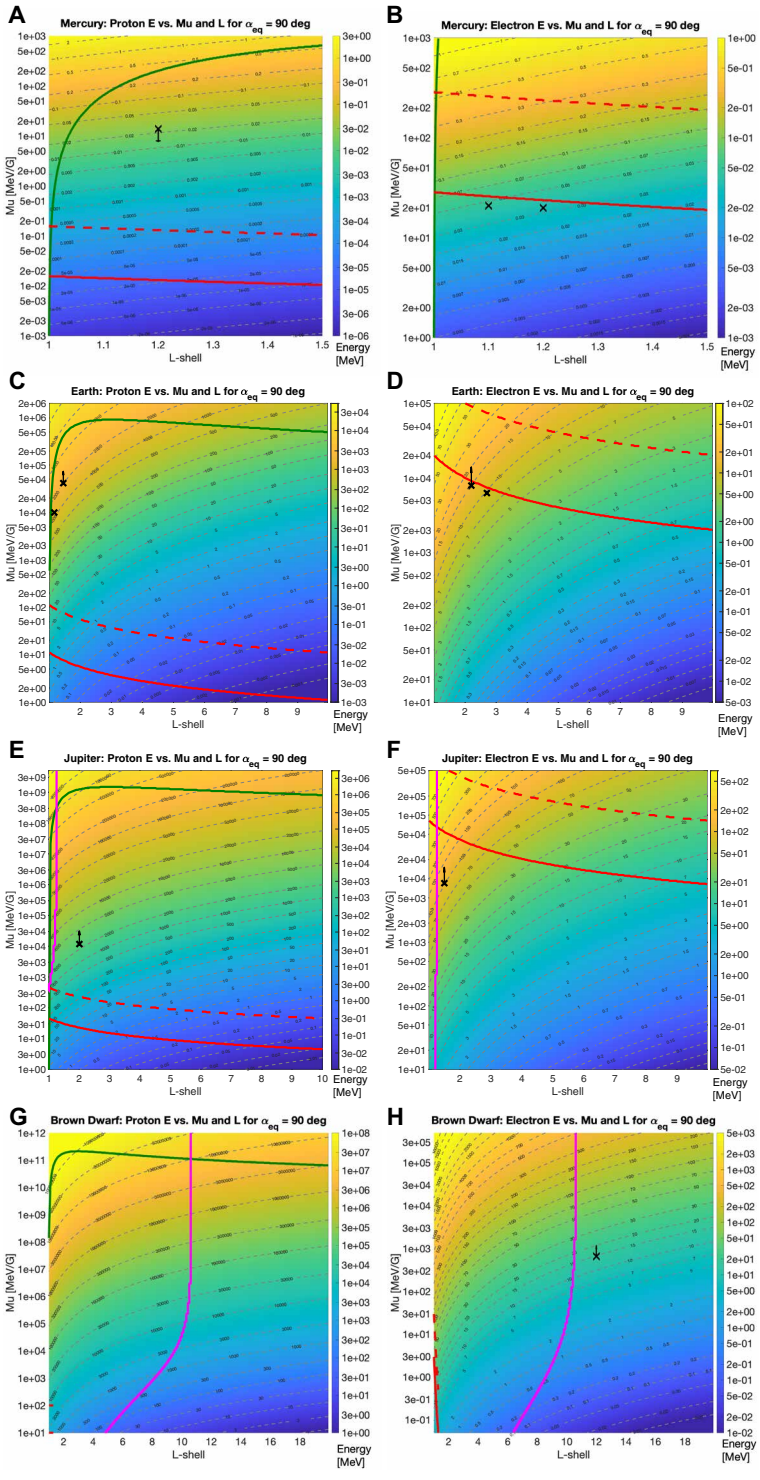

Fig. 2. Model results for other example planetary and brown dwarf systems. Energy limit model results applied to four different systems: Mercury (**A** and **B**), Earth (**C** and **D**), Jupiter (**E** and **F**), and ultracool brown dwarf LSRJ1835+3259 (**G** and **H**). Results for each plot are shown in the same format as in Fig. 1. For each of the four systems, results are shown for protons in the column on the left (A, C, E, G) and electrons in the column on the right (B, D, F, H). Actual observed limits are shown with black "x"s, with integral energy values shown with an upward arrow and uppermost limits shown with a downward arrow. For each system, we only show one or two of the highest energies reported at the lowest L-shells.

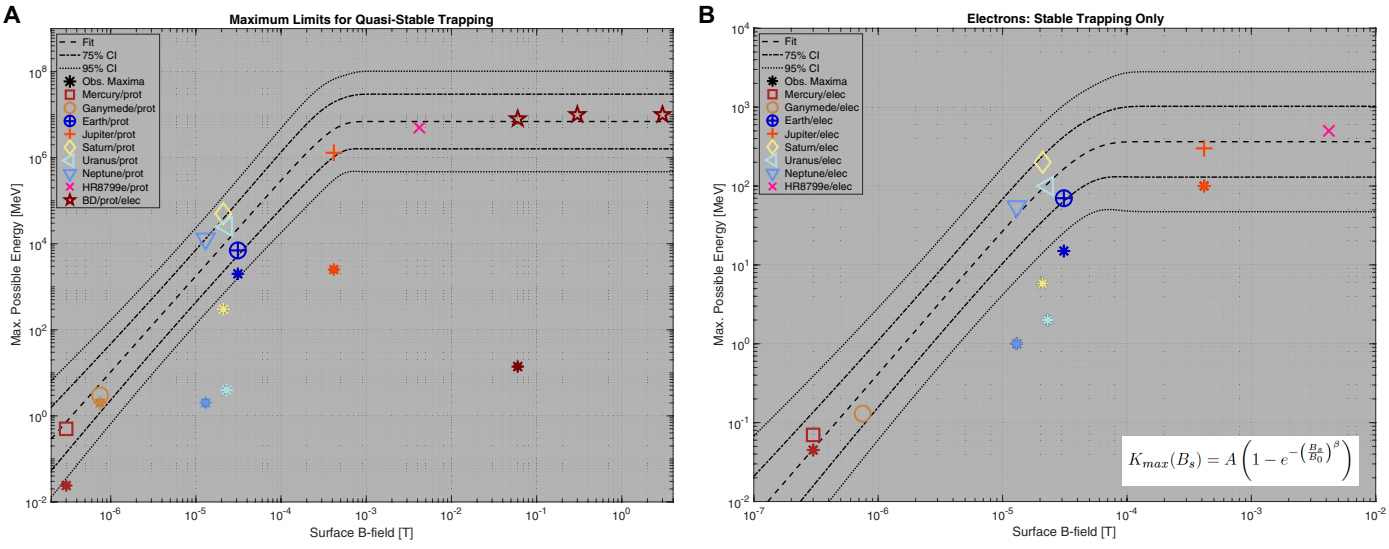

Fig. 3. Summary of model results showcasing the predicted upper energy asymptote. (**A**) Modeled maximum energy limits for ions (protons for all system plus also electrons at the brown dwarf systems) for quasi-stable trapping regimes in radiation belt systems throughout the Solar System and beyond. (**B**) Modeled energy limits for stably trapped electrons in various systems. Observational limits (as also noted in Fig. 2) are also shown with asterisks. Maximum possible energies in each system are plotted versus surface *B* field strength, which nicely organizes the data into a functional form with a power law at lower K_{max} and B_s and a rollover into an asymptotic limit in K_{max}, which is ultimately limited by the coupled intersection between the gyrosounding and synchrotron limits as a function of L and Mu in each system. The functional form for the fits is shown with the equation in the bottom right corner of (B), with the least-squares best fits (in log space) shown with the dashed black lines and the 75% and 95% confidence intervals on each fit shown with the dash dot and dotted lines, respectively. For the fits, the following constants are applied: ions: $A = 6.9 \pm 1.6$ TeV, $B_0 = 4.1 \pm 0.9 \times 10^{-4}$ T, $\beta = 2.2 \pm 0.5$; electrons: $A = 365 \pm 51$ MeV, $B_0 = 4.1 \pm 0.6 \times 10^{-5}$ T, $\beta = 1.8 \pm 0.3$, where *A* is the asymptotic limit of K_{max}, B_0 is the rollover point in B_s, and β is the slope on the power law.

factors, the model successfully reproduces a synchrotron emission boundary at $L \sim 11$ and quasi-stable electrons (i.e., $\kappa^2 < 1$) at 15 MeV, as seen in Fig. 2. When other brown dwarf systems are examined with this model using a reasonable range of stellar radii (0.7 to 1.4 $R_{Jupiter}$) and surface field strengths (order of 10^{-2} to 10^{0} T), the uppermost energy limit for both electrons and protons, which is ultimately bounded by the intersection of the synchrotron and gyrosounding thresholds, asymptotes at 7 TeV, as shown in Fig. 3.

Figure 3 demonstrates how the uppermost, quasi-stable trapping limits successfully bound all of the radiation belt systems with observations, and for electrons at most systems (with the notable exceptions of Ganymede and the brown dwarf, as discussed below), the stable trapping limit appears to be the ultimate limiting threshold. Note that the rotation rate of a system affects the rigidity loss term, which is mass dependent and dictates the stable trapping results (shown in Fig. 3B); so while protons at Neptune, Uranus, and the ultracool brown dwarf shown in Fig. 3A appear to be below the stable trapping limits in Fig. 3B, the mass dependence of the loss term and rapid rotation of those systems results in those protons being above the stable trapping limit for protons (not shown in Fig. 3B) and into the quasi-stable regime. This model implies that planetary and brown dwarf radiation belt systems may serve as sources of cosmic ray protons and electrons up to at most 7 TeV.

Figure 3 shows how the model predicts that the distribution of uppermost energy limits for each system sorts very nicely as a function of surface B field strength, B_s. The distribution is fit very well by a functional form (shown on Fig. 3) incorporating a power law at lower B_s and an asymptote around 7 TeV due to the coupled relationships between ρ, R_p, B_s, Mu, and *L* considering only the gyrosounding and synchrotron limits. Essentially, as B_s increases beyond the critical limit specified by B_0, the intersection of the gyrosounding and synchrotron limits moves to higher *L*-shells because of the dependency on the drift periods; as demonstrated here for a representative range of exoplanet and brown dwarf magnetic fields (Fig. 3), this results in an asymptote for K_{max} at ~7 TeV for both electrons and protons. As shown in the methods section, this relationship of K_{max} as a function of B_s, including the power law at lower K_{max} and maximum energy limit due to synchrotron energy loss, can also be derived from first principles using a combination of radial diffusion and synchrotron energy losses in a magnetospheric system ultimately limited by R_p and B_s. This analytical approach also produces the same power law as the model shown in Fig. 3: $\beta = +2.1$ from the analytical and $\beta = +2.2 \pm 0.5$ from the fit on Fig. 3. Ultimately, this model offers both predictive capability and a natural maximum energy limit attainable by planetary and brown dwarf radiation belt systems.

DISCUSSION

These results imply that radiation belt systems from the most extreme planetary systems (Jupiter, exoplanets) and brown dwarves may contribute to the cosmic ray spectrum up to ~7 TeV, but anything above that energy limit must be accelerated in some other type of system (e.g., supernova shocks, pulsars, magnetars, active galactic nuclei, etc.). This insight introduces many potential additional and nearby sources for the highest energy cosmic ray electrons ever observed (up to several teraelectron volts) and an explanation for the knee in the electron cosmic ray spectrum at ~1 TeV (*28*), a result recently supported by high-statistics measurements (*7*). Recent results attempting to explain the knee in the electron cosmic ray spectrum (*8*) concluded that it is likely due to a sudden change in abundance of

source systems, entirely consistent with the implications of this study: There are substantially more brown dwarfs in the Milky Way than there are pulsars, magnetars, supernova remnants, or other potential sources of electrons (and positrons) on the order of several teraelectron volts. We stress here that this is a previously unexplored hypothesis resulting from this study: Radiation belt systems at large (exo) planets and brown dwarf magnetospheres might provide an abundance of sources of electrons of up to approximately several teraelectron volts to contribute to the cosmic ray spectrum; however, that hypothesis should be evaluated and tested through future work, particularly considering losses to the outer boundary of systems and how those particles might escape into interstellar space.

This simple yet effective predictive model can also be applied to exoplanetary systems. Figure 1 shows the example for protons at exoplanet HR-8799-e (*29*). This gas giant planet orbits F-type star HR 8799 at an estimated distance of 16.4 astronomical unit (au) and has a mass of 10× that of Jupiter. Assuming that it has a comparably strong surface B field of ~40 G, a plasma density and radius comparable to Jupiter, R_H ~ 1.2 R_J, and a spin period of around 1 hour, HR-8799-e is capable of stably trapping electrons up to 500 MeV and quasi-stably trapping protons up to 5 TeV. Most importantly from an astronomical perspective, if HR-8799-e's magnetosphere is a radiation belt system as estimated here, then it should also be emitting significant synchrotron emissions, which might render it as a particular target of interest for future observational campaigns. With the model tuned as described above, we predict peak electron synchrotron emissions around L ~ 3.6. Using the NASA Exoplanet Archive, we applied our model to 25 large (≥6 Earth masses) exoplanets that orbit their host stars at >0.5 au and are within ~42 light years (ly) of Earth and of those 17 are potentially synchrotron emitters, which we have ordered by a detectability proxy as described and listed in the Supplementary Materials This demonstrates how this simple model can also be used to identify potential exoplanets of interest, not only from an observational perspective (*30*) but also concerning star/planet interactions (*31*), atmospheric evolution (*32*) and habitability, since radiation levels within a planetary system are a factor of consideration for sustaining life (*33*, *34*).

MATERIALS AND METHODS

Table 1 details the model parameters used for each planetary and brown dwarf magnetosphere and the corresponding maximum energies, both observed (with references for each observation listed below the table) and predicted by the model. These results correspond to those shown in Fig. 3.

The following equations were used to develop the model that generated the results presented in this study.

The relativistic first adiabatic invariant is calculated as

$$\mathrm{Mu} = \frac{K_\perp\left(K_\perp + 2m_0c^2\right)}{2Bm_0c^2} \quad (1)$$

where $K_\perp$ is particle kinetic energy perpendicular to B.

For gyrosounding and rigidity, the following is used for the relativistic gyroradius and rigidity parameter, κ

$$\text{Gyroradius:}\quad \rho = \frac{\gamma m_0 v \sin\alpha}{qB} \quad (2)$$

Table 1. Summary of results and key model parameters. References for observations at each system include: Mercury/protons (*35*), Mercury/electrons (*35*, *36*), Earth/protons (*1*, *37*), Earth/electrons (*2*, *38*), Jupiter/protons (*3*), Jupiter/electrons (*4*), Ganymede/protons and /electrons (*39*), Saturn/protons (*25*, *40*), Uranus/protons (*41*) and /electrons (*42*, *43*), Neptune/protons (*41*) and /electrons (*43*, *44*), and ultracool brown dwarf /electrons (*5*, *6*, *26*).

Magnetospheric system	Body radius	Dipole strength (B_s)	Rotation period	Plasma density	Max energy observed	Max energy predicted	Regime
[]	[km]	[T]	[hours]	[#/cm^3]	[MeV]	[MeV]	[]
Mercury	2,440	3.00E−07	1407.500	1E+02	Elec: 4.5E−02	Elec: 7E−02	Stable
					Prot: 2.4E−02	Prot: 5E−01	Quasi-stable
Earth	6,371	3.11E−05	23.934	1E+02	Elec: ≥1.5E+01	Elec: 7E+01	Stable
					Prot: ≥2.0E+03	Prot: 7E+03	Quasi-stable
Jupiter	6,9950	4.17E−04	9.925	1E+02	Elec: ≥1.0E+02	Elec: 3E+02	Stable
					Prot: ≥2.5E+03	Prot: 1E+06	Quasi-stable
Ganymede	2,631	7.50E−07	171.720	1E+02	Elec: ≥2.0E+00	Elec: 1E−01	Quasi-stable
					Prot: ≥2.0E+00	Prot: 3E+00	Quasi-stable
Saturn	58,300	2.10E−05	10.561	8E+01	Elec: 5.8E+00	Elec: 2E+02	Stable
					Prot: 3.0E+02	Prot: 5E+04	Quasi-stable
Uranus	25,360	2.30E−05	17.240	7E−01	Elec: 2.0E+00	Elec: 1E+02	Stable
					Prot: 4.0E+00	Prot: 3E+04	Quasi-stable
Neptune	24,600	1.30E−05	16.110	4E−02	Elec: 1.0E+00	Elec: 6E+01	Stable
					Prot: 2.0E+00	Prot: 1E+04	Quasi-stable
HR-8799-e	84,000	4.20E−03	9.000	2E+03	Unobserved	Elec: 5E+02	Unobserved
						Prot: 8E+06	
LSRJ1835 + 3295	70,000	6.00E−02	1–3	1E+00	Elec: >14 MeV	Elec: 1E+07	Quasi-stable
					Prot: Unobserved	Prot: 1E+07	Quasi-stable

$$\text{Rigidity parameter: } \kappa^2 = \frac{R_{cB}}{\rho} \tag{3}$$

where γ is the Lorentz factor with m_0 the rest mass; v, q, and α are the particle's velocity, charge, and pitch angle, respectively; B is the magnetic field strength; and R_{cB} is the radius of curvature of the magnetic field lines (calculated from a dipole) for the rigidity parameter.

For the adjustment of magnetic radius of curvature for rapidly spinning magnetospheres, the radius of curvature of the magnetic field is adjusted to account for pressure balance between the rotating, mass-loaded field lines pulling outward against the magnetic curvature pulling back inward using the following equation

$$R_{cB\Omega} = \frac{B}{4\pi\mu_0\left(n\Omega^2 r\right)} + \frac{3M_B^2}{\mu_0 r^7} \tag{4}$$

where $R_{cB\Omega}$ is the radius of curvature of the B field accounting for the spinning system, n is the plasma density in the system, Ω is the planetary rotation frequency, M_B is the magnetic moment of the planet, and r is the radial distance from the planet center to the test location along the L-shell (assumed in the rotational equatorial plane).

Synchrotron energy loss rate is calculated with

$$f_\rho K_{sync} = 88.46 \times 10^{-3}\left(\frac{K^4}{\rho}\right) \tag{5}$$

with K in [GeV] and ρ in [m], yielding energy loss per gyroperiod in [keV/T_ρ], where T_ρ is the gyroperiod in [s].

Particle drift periods as a function of energy and L-shell are calculated with the following model described in (*10*)

$$f_D = \frac{3}{2\pi}\left(\gamma^2 - 1\right)\frac{m_0 c^2 L}{\gamma q B R_\rho^2}\left(\frac{D_y}{T_y}\right) \tag{6}$$

where

$$T_0 - 1 + \frac{1}{2\sqrt{3}}\log\left(2+\sqrt{3}\right) \tag{7}$$

$$T_1 = \frac{\pi}{6\sqrt{2}} \tag{8}$$

$$D_y = \frac{1}{12}\left\{4T_0 - \left(3T_0 - 5T_1\right)\sin\alpha - \left(T_0 - T_1\right)\left[\sin\alpha\log(\sin\alpha) + \sqrt{\sin\alpha}\right]\right\} \tag{9}$$

$$T_y = T_0 - \frac{1}{2}\left(T_0 - T_1\right)(\sin\alpha)^{\frac{3}{2}} \tag{10}$$

For additional details, including estimations for the most likely targets of synchrotron emitting exoplanets in the nearby galactic vicinity, see the Supplementary Materials.

Supplementary Materials

This PDF file includes:

Supplementary Text
Figs. S1 to S15
Table S1
Software for model and figure generation
References

REFERENCES

1. J. E. Mazur, T. P. O'Brien, M. D. Looper, The relativistic proton spectrometer: A review of sensor performance, applications, and science. *Space Sci. Rev.* **219**, 26 (2023).
2. J. B. Blake, W. A. Kolasinski, R. W. Fillius, E. G. Mullen, Injection of electrons and protons with energies of tens of MeV into L < 3 on 24 March 1991. *Geophys. Res. Lett.* **19**, 821–824 (1992).
3. P. Kollmann, G. Clark, C. Paranicas, B. Mauk, E. Roussos, Q. Nénon, H. B. Garrett, A. Sicard, D. Haggerty, A. Rymer, Jupiter's ion radiation belts inward of Europa's orbit. *J. Geophys. Res.* **126**, e2020JA028925 (2021).
4. I. de Pater, D. E. Dunn, VLA observations of Jupiter's synchrotron radiation at 15 and 22 GHz. *Icarus* **163**, 449–455 (2003).
5. M. M. Kao, A. J. Mioduszewski, J. Villadsen, E. L. Shkolnik, Resolved imaging confirms a radiation belt around an ultracool dwarf. *Nature* **619**, 272–275 (2023).
6. J. B. Climent, J. C. Guirado, M. Pérez-Torres, J. M. Marcaide, L. Peña-Moñino, Evidence for a radiation belt around a brown dwarf. *Science* **381**, 1120–1124 (2023).
7. F. Aharonian, F. A. Benkhali, J. Aschersleben, H. Ashkar, M. Backes, V. B. Martins, R. Batzofin, Y. Becherini, D. Berge, K. Bernlöhr, B. Bi, M. Böttcher, C. Boisson, J. Bolmont, M. de Bony de Lavergne, J. Borowska, M. Bouyahiaoui, R. Brose, A. Brown, F. Brun, B. Bruno, T. Bulik, C. Burger-Scheidlin, T. Bylund, S. Casanova, J. Celic, M. Cerruti, T. Chand, S. Chandra, A. Chen, J. Chibueze, O. Chibueze, T. Collins, G. Cotter, J. D. Mbarubucyeye, J. Devin, J. Djuvsland, A. Dmytriiev, K. Egberts, S. Einecke, J.-P. Ernenwein, S. Fegan, K. Feijen, G. Fontaine, S. Funk, S. Gabici, Y. A. Gallant, J. F. Glicenstein, J. Glombitza, G. Grolleron, B. Heß, W. Hofmann, T. L. Holch, M. Holler, D. Horns, Z. Huang, M. Jamrozy, F. Jankowsky, V. Joshi, I. Jung-Richardt, E. Kasai, K. Katarzynski, D. Kerszberg, R. Khatoon, B. Khelifi, W. Kluzniak, N. Komin, K. Kosack, D. Kostunin, A. Kundu, R. G. Lang, S. Le Stum, F. Leitl, A. Lemiere, M. Lemoine-Goumard, J.-P. Lenain, F. Leuschner, A. Luashvili, J. Mackey, D. Malyshev, D. Malyshev, V. Marandon, P. Marinos, G. Marti-Devesa, R. Marx, M. Meyer, A. Mitchell, R. Moderski, M. O. Moghadam, L. Mohrmann, A. Montanari, E. Moulin, M. de Naurois, J. Niemiec, S. Ohm, L. Olivera-Nieto, E. de Ona Wilhelmi, M. Ostrowski, S. Panny, M. Panter, D. Parsons, U. Pensec, G. Peron, G. Pühlhofer, M. Punch, A. Quirrenbach, S. Ravikularaman, M. Regeard, A. Reimer, O. Reimer, I. Reis, H. Ren, B. Reville, F. Rieger, G. Rowell, B. Rudak, E. Ruiz-Velasco, V. Sahakian, H. Salzmann, A. Santangelo, M. Sasaki, J. Schäfer, F. Schüssler, H. M. Schutte, J. N. S. Shapopi, A. Sharma, H. Sol, S. Spencer, L. Stawarz, S. Steinmassl, C. Steppa, H. Suzuki, T. Takahashi, T. Tanaka, A. M. Taylor, R. Terrier, M. Tsirou, C. van Eldik, M. Vecchi, C. Venter, J. Vink, T. Wach, S. J. Wagner, A. Wierzcholska, M. Zacharias, A. A. Zdziarski, A. Zech, N. Zywucka, High-statistics measurement of the cosmic-ray electron spectrum with H.E.S.S. *Phys. Rev. Lett.* **133**, 221001 (2024).
8. S. Thoudam, Origin of the break in the cosmic-ray electron plus positron spectrum at ~1 TeV. *Astron. Astrophys.* **690**, A351 (2024).
9. T. G. Northrop, Adiabatic charged-particle motion. *Rev. Geophys.* **1**, 283–304 (1963).
10. M. Schulz, L. J. Lanzerotti, *Particle diffusion in the radiation belts, in Physics and Chemistry in Space* (Springer, 1974), vol. 7.
11. R. M. Millan, R. M. Thorne, Review of radiation belt relativistic electron loss. *J. Atmos. Sol. Terr. Phys.* **69**, 362–377 (2007).
12. Y. Y. Shprits, D. A. Subbotin, N. P. Meredith, S. R. Elkington, Review of modeling of losses and sources of relativistic electrons in the outer radiation belt II: Local acceleration and loss. *J. Atmos. Sol. Terr. Phys.* **70**, 1694–1713 (2008).
13. W. Li, M. K. Hudson, Earth's Van Allen radiation belts: From discovery to the Van Allen Probes era. *J. Geophys. Res.* **124**, 8319–8351 (2019).
14. P. C. Gray, L. C. Lee, Particle pitch angle diffusion due to nonadiabatic effects in the plasma sheet. *J. Geophys. Res.* **87**, 7445–7452 (1982).
15. A. Masters, C. Ioannou, N. Rayns, Does Uranus' asymmetric magnetic field produce a relatively weak proton radiation belt? *Geophys. Res. Lett.* **49**, e2022GL100921 (2022).
16. W. Tu, X. Li, Adiabatic effects on radiation belt electrons at low altitude. *J. Geophys. Res.* **116**, 10.1029/2011JA016468 (2011).
17. N. Achilleos, P. Guio, F. Hardy, C. Paranicas, A. M. Sorba, The magnetodisk regions of Jupiter and Saturn, in *Magnetospheres in the Solar System*, R. Maggiolo, N. André, H. Hasegawa, and D. T. Welling, Eds. (John Wiley & Sons Inc, 2021), pp. 437–452.
18. T. W. Speiser, Particle trajectories in model current sheets: 1. Analytical solutions. *J. Geophys. Res.* **70**, 4219–4226 (1965).
19. V. Sergeev, E. Sazhina, N. Tsyganenko, J. Lundblad, F. Soraas, Pitch-angle scattering of energetic protons in the magnetotail current sheet as the dominant source of their isotropic precipitation into the nightside ionosphere. *Planet. Space Sci.* **31**, 1147–1155 (1983).
20. J. Buchner, L. M. Zelenyi, Deterministic chaos in the dynamics of charged particles near a magnetic field reversal. *Phys. Lett. A* **118**, 395–399 (1986).
21. M. Ashour-Abdalla, J. Berchem, J. Buchner, L. M. Zelenyi, Large and small scale structures in the plasma sheet: A signature of chaotic motion and resonance effects. *Geophys. Res. Lett.* **18**, 1603–1606 (1991).
22. C. Wilkins, V. Angelopoulos, A. Runov, A. Artemyev, X.-J. Zhang, J. Liu, E. Tsai, Statistical characteristics of the electron isotropy boundary. *J. Geophys. Res.* **128**, e2023JA031774 (2023).

23. G. Clark, P. Kollmann, B. H. Mauk, C. Paranicas, D. Haggerty, A. Rymer, H. T. Smith, J. Saur, F. Allegrini, S. Duling, R. W. Ebert, W. S. Kurth, R. Gladstone, T. K. Greathouse, W. Li, F. Bagenal, J. E. P. Connerney, S. Bolton, J. R. Szalay, A. H. Sulaiman, C. J. Hansen, D. L. Turner, Energetic charged particle observations during Juno's close flyby of Ganymede. *Geophys. Res. Lett.* **49**, e2022GL098572 (2022).
24. P. Kollmann, I. Cohen, R. C. Allen, G. Clark, E. Roussos, S. Vines, W. Dietrich, J. Wicht, I. de Pater, K. D. Runyon, R. Cartwright, A. Masters, D. Brain, K. Hibbits, B. Mauk, M. Gkioulidou, A. Rymer, R. McNutt Jr., V. Hue, S. Stanley, P. Brandt, Magnetospheric studies: A requirement for addressing interdisciplinary mysteries in the Ice Giant systems. *Space Sci. Rev.* **216**, 78 (2020).
25. E. Roussos, P. Kollmann, N. Krupp, A. Kotova, L. Regoli, C. Paranicas, D. G. Mitchell, S. M. Krimigis, D. Hamilton, P. Brandt, J. Carbary, S. Christon, K. Dialynas, I. Dandouras, M. E. Hill, W. H. Ip, G. H. Jones, S. Livi, B. H. Mauk, B. Palmaerts, E. C. Roelof, A. Rymer, N. Sergis, H. T. Smith, A radiation belt of energetic protons located between Saturn and its rings. *Science* **362**, eaat1962 (2018).
26. P. A. Miles-Páez, M. Stanimir, G. Benjamin, The photometric periods of rapidly rotating field ultra-cool dwarfs. *Mon. Not. R. Astron. Soc.* **521**, 952–968 (2023).
27. J. Saur, C. Willmes, C. Fischer, A. Wennmacher, L. Roth, A. Youngblood, D. F. Strobel, A. Reiners, Brown dwarfs as ideal candidates for detecting UV aurora outside the Solar System: *Hubble* Space Telescope observations of 2MASS J1237+6526. *Astron. Astrophys.* **655**, A75 (2021).
28. A. Archer, W. Benbow, R. Bird, R. Brose, M. Buchovecky, J. H. Buckley, V. Bugaev, M. P. Connolly, W. Cui, M. K. Daniel, Q. Feng, J. P. Finley, L. Fortson, A. Furniss, G. Gillanders, M. Hütten, D. Hanna, O. Hervet, J. Holder, G. Hughes, T. B. Humensky, C. A. Johnson, P. Kaaret, P. Kar, N. Kelley-Hoskins, M. Kertzman, D. Kieda, M. Krause, F. Krennrich, S. Kumar, M. J. Lang, T. T. Y. Lin, G. Maier, S. McArthur, P. Moriarty, R. Mukherjee, S. O'Brien, R. A. Ong, A. N. Otte, A. Petrashyk, M. Pohl, E. Pueschel, J. Quinn, K. Ragan, P. T. Reynolds, G. T. Richards, E. Roache, C. Rulten, I. Sadeh, M. Santander, G. H. Sembroski, D. Staszak, I. Sushch, S. P. Wakely, R. M. Wells, P. Wilcox, A. Wilhelm, D. A. Williams, T. J. Williamson, B. Zitzer, VERITAS Collaboration, Measurement of cosmic-ray electrons at TeV energies by VERITAS. *Phys. Rev. D* **98**, 062004 (2018).
29. S. Lacour, M. Nowak, J. Wang, O. Pfuhl, F. Eisenhauer, R. Abuter, A. Amorim, N. Anugu, M. Benisty, J. P. Berger, H. Beust, N. Blind, M. Bonnefoy, H. Bonnet, P. Bourget, W. Brandner, A. Buron, C. Collin, B. Charnay, F. Chapron, Y. Clénet, V. Coudé, du Foresto, P. T. de Zeeuw, C. Deen, R. Dembet, J. Dexter, G. Duvert, A. Eckart, N. M. Förster Schreiber, P. Fédou, P. Garcia, R. Garcia Lopez, F. Gao, E. Gendron, R. Genzel, S. Gillessen, P. Gordo, A. Greenbaum, M. Habibi, X. Haubois, F. Haußmann, T. Henning, S. Hippler, M. Horrobin, Z. Hubert, A. Jimenez Rosales, L. Jocou, S. Kendrew, P. Kervella, J. Kolb, A.-M. Lagrange, V. Lapeyrère, J.-B. Le Bouquin, P. Léna, M. Lippa, R. Lenzen, A.-L. Maire, P. Mollière, T. Ott, T. Paumard, K. Perraut, G. Perrin, L. Pueyo, S. Rabien, A. Ramírez, C. Rau, G. Rodríguez-Coira, G. Rousset, J. Sanchez-Bermudez, S. Scheithauer, N. Schuhler, O. Straub, C. Straubmeier, E. Sturm, L. J. Tacconi, F. Vincent, E. F. van Dishoeck, S. von Fellenberg, I. Wank, I. Waisberg, F. Widmann, E. Wieprecht, M. Wiest, E. Wiezorrek, J. Woillez, S. Yazici, D. Ziegler, G. Zins, First direct detection of an exoplanet by optical interferometry. *Astron. Astrophys.* **623**, L11 (2019).
30. T. Lazio, Radio observations as an exoplanet discovery method, in *Handbook of Exoplanets*, H. J. Deeg and J. A. Belmonte, Eds. (Springer, 2017), pp. 2481–2495.
31. R. Ramstad, S. Barabash, Do intrinsic magnetic fields protect planetary atmospheres from stellar winds? *Space Sci. Rev.* **217**, 36 (2021).
32. G. Gronoff, P. Arras, S. Baraka, J. M. Bell, G. Cessateur, O. Cohen, S. M. Curry, J. J. Drake, M. Elrod, J. Erwin, K. Garcia-Sage, C. Garraffo, A. Glocer, N. G. Heavens, K. Lovato, R. Maggiolo, C. D. Parkinson, C. S. Wedlund, D. R. Weimer, W. B. Moore, Atmospheric escape processes and planetary atmospheric evolution. *J. Geophys. Res.* **125**, e2019JA027639 (2020).
33. J.-M. Grießmeier, F. Tabataba-Vakili, A. Stadelmann, J. L. Grenfell, D. Atri, Galactic cosmic rays on extrasolar Earth-like planets I. Cosmic ray flux. *Astron. Astrophys.* **581**, A44 (2015).
34. P. E. Driscoll, Planetary interiors, magnetic fields, and habitability, in *Handbook of Exoplanets*, H. J. Deeg and J. A. Belmonte, Eds. (Springer, 2018), pp. 1165–1184.
35. B. M. Walsh, A. S. Ryou, D. G. Sibeck, I. I. Alexeev, Energetic particle dynamics in Mercury's magnetosphere. *J. Geophys. Res. Space Phys.* **118**, 1992–1999 (2013).
36. G. C. Ho, S. M. Krimigis, R. E. Gold, D. N. Baker, B. J. Anderson, H. Korth, J. A. Slavin, R. L. McNutt Jr., R. M. Winslow, S. C. Solomon, Spatial distribution and spectral characteristics of energetic electrons in Mercury's magnetosphere. *J. Geophys. Res. Space Phys.* **117**, 10.1029/2012JA017983 (2012).
37. A. Bruno, High-energy trapped protons measured by PAMELA, paper presented at the IRENE Space Radiation Modeling and Data Analysis Workshop, 29 to 31 May 2019, Sykia, Greece (2019).
38. D. N. Baker, A. N. Jaynes, V. C. Hoxie, R. M. Thorne, J. C. Foster, X. Li, J. F. Fennell, J. R. Wygant, S. G. Kanekal, P. J. Erickson, W. Kurth, W. Li, Q. Ma, Q. Schiller, L. Blum, D. M. Malaspina, A. Gerrard, L. J. Lanzerotti, An impenetrable barrier to ultrarelativistic electrons in the Van Allen radiation belts. *Nature* **515**, 531–534 (2014).
39. P. Kollmann, G. Clark, C. Paranicas, B. Mauk, D. Haggerty, A. Rymer, F. Allegrini, Ganymede's Radiation Cavity and Radiation Belts. *Geophys. Res. Lett.* **49**, e2022GL098474 (2022).
40. N. Krupp, E. Roussos, A. Lagg, J. Woch, A. L. Müller, S. M. Krimigis, D. G. Mitchell, E. C. Roelof, C. Paranicas, J. Carbary, G. H. Jones, D. C. Hamilton, S. Livi, T. P. Armstrong, M. K. Dougherty, N. Sergis, Energetic particles in Saturn's magnetosphere during the Cassini nominal mission (July 2004–July 2008). *Planet. Space Sci.* **57**, 1754–1768 (2009).
41. B. H. Mauk, Comparative investigation of the energetic ion spectra comprising the magnetospheric ring currents of the solar system. *J. Geophys. Res. Space Phys.* **119**, 9729–9746 (2014).
42. B. H. Mauk, S. M. Krimigis, E. P. Keath, A. F. Cheng, T. P. Armstrong, L. J. Lanzerotti, G. Gloeckler, D. C. Hamilton, The hot plasma and radiation environment of the Uranian magnetosphere. *J. Geophys. Res. Space Phys.* **92**, 15283–15308 (1987).
43. B. H. Mauk, N. J. Fox, Electron radiation belts of the solar system. *J. Geophys. Res. Space Phys.* **115**, 10.1029/2010JA015660 (2010).
44. S. M. Krimigis, B. H. Mauk, A. F. Cheng, E. P. Keath, M. Kane, T. P. Armstrong, G. Gloeckler, L. J. Lanzerotti, Hot plasma parameters in Neptune's magnetosphere. *Geophys. Res. Lett.* **119**, 9729–9746 (2014).
45. L. Rybicki, *Radiative processes in astrophysics* (Wiley-Interscience, 1991).
46. S. Stanley, J. Bloxham, Convective region geometry as the cause of Uranus' and Neptune's unusual magnetic fields. *Nature* **428**, 151–153 (2004).
47. S. Stanley, J. Bloxham, Numerical dynamo models of Uranus' and Neptune's magnetic fields. *Icarus* **184**, 556–572 (2006).
48. A. Osmane, E. Kilpua, H. George, O. Allanson, M. Kalliokoski, Radial Transport in the Earth's Radiation Belts: Linear, Quasi-linear, and Higher-order Processes. *Astrophys. J. Suppl.* **269**, 44 (2023).
49. C.-G. Fälthammar, Effects of time-dependent electric fields on geomagnetically trapped radiation. *J. Geophys. Res. Space Phys.* **70**, 2503–2516 (1965).
50. A. Osmane, J. K. Sandhu, T. Elsden, O. Allanson, L. Turc, Radial Diffusion Driven by Spatially Localized ULF Waves in the Earth's Magnetosphere. *J. Geophys. Res. Space Phys.* **130**, e2024JA033393 (2025).
51. G. I. Barenblatt, *Scaling, Self-Similarity, and Intermediate Asymptotics: Dimensional Analysis and Intermediate Asymptotics* (Cambridge Univ. Press, 1996).
52. Y. Cendes, E. Berger, K. D. Alexander, S. Gomez, A. Hajela, R. Chornock, T. Laskar, R. Margutti, B. Metzger, M. F. Bietenholz, A Mildly Relativistic Outflow Launched Two Years after Disruption in Tidal Disruption Event AT2018hyz. *Astrophys. J.* **938**, 28 (2022).

Acknowledgments: D.L.T. is thankful to the National Science Foundation (NSF) for funding that enabled this research. **Funding:** D.L.T. acknowledges funding from National Science Foundation grant S03464-01. S.R. acknowledges funding form the Johns Hopkins University Applied Physics Laboratory Independent R&D fund. **Author contributions:** Conceptualization: D.L.T., A.Y.U., G.C., L.R., A.E., and T.N. Methodology: D.L.T., A.O., G.C., S.R., T.N., and L.R. Investigation: D.L.T., G.C., T.N., L.R., and S.R. Visualization: D.L.T. Supervision: D.L.T. Writing—original draft: D.L.T. and G.C. Writing—review and editing: D.L.T., S.R., A.O., A.E., G.C., T.N., and L.R. Resources: D.L.T., S.R., G.C., and A.E. Validation: D.L.T., L.R., G.C., and A.E. Data curation: D.L.T. and G.C. Funding acquisition: D.L.T. Formal analysis: D.L.T., L.R., and A.E. Software: D.L.T. Project administration: D.L.T. **Competing interests:** The authors declare that they have no competing interests. **Data, code, and materials availability:** All data and code needed to evaluate and reproduce the results in the paper are present in the paper and/or the Supplementary Materials. Please contact the corresponding author for access to materials generated by this study.

Submitted 10 July 2025
Accepted 3 February 2026
Published 4 March 2026
10.1126/sciadv.aea4945

ScienceAdvances

Universal energy limits of radiation belts in planetary and brown dwarf magnetospheric systems

Drew L. Turner, Savvas Raptis, Adnane Osmane, Arika Egan, George Clark, Tom Nordheim, Leonardo Regoli, and Aleksandr Y. Ukhorskiy

Sci. Adv. **12** (10), eaea4945. DOI: 10.1126/sciadv.aea4945

Science Advances (ISSN 2375-2548) is published by the American Association for the Advancement of Science. 1200 New York Avenue NW, Washington, DC 20005. The title *Science Advances* is a registered trademark of AAAS.